Phase transformation behavior in a multipurpose dental casting gold alloy during continuous heating

H. I. KIM, H. J. SEOL
Department of Dental Materials, College of Dentistry, Pusan National University, 1-10 Ami-dong, Seo-gu, Pusan 602-739, Korea

K. HISATSUNE, HTAIN-WINN, A. A. EI S. SAKRANA, Y. TAKUMA, K. KAWASAKI*
*Departments of Dental Materials Science and *Preventive Dentistry, Nagasaki University School of Dentistry, Nagasaki 852, Japan*

Phase transformation in a multipurpose dental casting gold alloy during continuous heating was studied by electrical resistivity measurements, hardness tests, X-ray diffraction and scanning and transmission electron microscopy. The behavior can be explained by the following reaction sequences in the nodule: $\alpha_1(\mathrm{fcc}) + \alpha_2(\mathrm{L1_2}) \rightarrow \alpha_1(\mathrm{fcc}) + \alpha_2(\mathrm{L1_2}) + \beta(\mathrm{L1_0})$, where fcc is face centred cubic. A discontinuous precipitation with very fine nodules contributed to the hardening and the growth produced the softening. This multipurpose gold alloy is characterized by the introduction of a PtZn ordered phase with $\mathrm{L1_0}$ structure instead of a CuAu I phase.

1. Introduction

It is well known that gold alloy is one of the most useful materials in dentistry. Gold alloys with different compositions have been commercially produced for applications in many kinds of prosthesis. Use of the same alloy in an oral environment is ideally applicable owing to its corrosion resistance. However, each appliance demands different strength and properties. The required strength is aquired by age-hardening. The CuAu I ordered phase with $\mathrm{L1_0}$ structure for inlays, clasps, crowns, bridges and dentures [1–4] and the ordered phase with face-centred cubic (fcc) structure for porecelain metal [5–7] play an important role in hardening. Recently, a multipurpose alloy was produced that covered all applications. It has been reported that this alloy seemed to be suitable in dental prosthesis [8–11]. Unfortunately, no studies have been made of the age-hardening behavior in this multipurpose alloy.

The aim of the present study is to clarify the phase transformation behavior in a multipurpose dental gold alloy during continuous heating by using electrical resistivity measurements, hardness tests, X-ray diffraction (XRD), and scanning and transmission electron microscopy (SEM and TEM).

2. Materials and methods

The specimen used in this study was a multipurpose dental gold alloy with 60.5 Au–13.8 Ag–11.2 Cu–7.5 Pt–4.9 Zn–2.0 In–0.1 Ir (at %). Degunorm, Degussa AG, Hanau, Germany).

Sheets 0.5 and 0.1 mm thick were prepared by alternate rolling and annealing for use in the hardness tests and for other experiments, respectively. These specimens were solution-treated at 800 °C for 60 min under an argon atmosphere and then quenched into ice brine. Subsequently, anisothermal annealing at heating rates of 5, 2, 1, 0.5 or 0.2 °C $\mathrm{min^{-1}}$ from room temperature to 800 °C in vacuo was performed.

The hardness tests were made using a Vickers hardness indenter with a 300 g load. The resistivity measurements were made using a direct current (d.c.) potentiometric method with four probes. Structural changes were examined by XRD and TEM. For the XRD, minus-300 mesh powder was prepared from the alloy by filing. The powdered specimens, in an evacuated silica tube, were solution-treated and annealed. XRD (RAD-rA, Rigaku Corp., Tokyo, Japan) was employed using graphite monochromatized CuK_α radiation with 50 kV and 150 mA. Specimens for SEM analysis were prepared using a standard metallographic technique, with final etching achieved with a freshly prepared aqueous solution of 10% KCN and 10% $(\mathrm{NH_4})_2\mathrm{S_2O_8}$. For TEM, discs 3 mm in diameter were punched out of the heat-treated sheets. They were electrothinned using a double-jet technique in a solution of 35 g $\mathrm{CrO_3}$, 200 ml of $\mathrm{CH_3COOH}$ and 10 ml of $\mathrm{H_2O}$. The SEM and TEM observations were performed at 20 kV (S-520, Hitachi Co., Tokyo, Japan) and 200 kV (H-800, Hitachi Co., Tokyo, Japan), respectively.

3. Results and discussion

3.1. Equilibrium phases

Fig. 1 shows the variation of normalized electrical resistivity and its temperature derivatives in the present

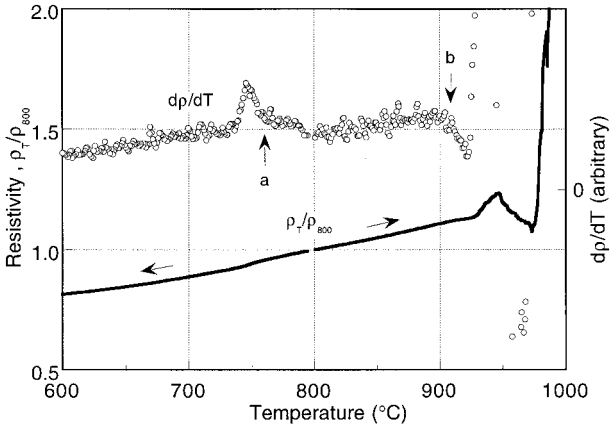

Figure 1 Variation of electrical resistivity and its temperature derivatives during cooling and heating at a rate of 0.5 °C min^{-1}.

alloy during continuous cooling from 800 °C to room temperature and subsequently during heating to 1000 °C at a rate of 0.5 °C min^{-1}. ρ_T and ρ_{800} are the resistivities at T and 800 °C, respectively. Two transition temperatures (765 and 907 °C) were found, as indicated by the arrows (a and b) in the figure. Considering the abnormal resistivity change for higher temperature ranges than 900 °C, the differential thermal analysis (DTA) data of Takada *et al*. [10] and that given in the manufacturer's brochure, 907 °C must correspond to the solidus temperature. A solid-state transition may occur at 765 °C. Fig. 2 shows XRD profiles in the specimens (a) quenched from 800 °C and (b) slowly cooled to room temperature. XRD analysis reveals that the equilibrium phases are two phases $(\alpha_1 + \alpha_2)$ at 800 °C and three phase $(\alpha_1 + \alpha_2 + \beta)$ at room temperature. The α_1 phase has an fcc structure with lattice parameters of $a_{200} = 0.401$ nm at 800 °C and $a_{200} = 0.402$ nm at 25 °C, the α_2 phase has an ordered fcc structure with $a_{200} = 0.395$ nm at 800 °C and $a_{200} = 0.396$ nm at 25 °C and the β phase has an ordered face-centred tetragonal (fct) structure with $a = 0.401$ nm and $c = 0.353$ nm. Judging from the composition and the lattice parameters, it is supposed that α_1 is a gold-rich phase and α_2 is a platinum-rich ordered phase. The latter is possibly an ordered phase based on Pt_3Zn or Pt_3In. According to the references, the lattice parameter of Pt_3Zn is 0.389 nm [12] and that of Pt_3In is 0.399 nm [13]. On the other hand, the β phase images PtZn with $L1_0$ structure. References [12, 14] have reported lattice parameters of $a = 0.404$ nm and $c = 0.347$ nm as PtZn phase with $L1_0$ structure. We obtained very close values in the present alloy. Takada *et al*. [10] have reported energy dispersive X-ray (EDX) analyses in cast samples of the same commercial alloy, which had been solution-treated or age-treated. According to their data, the atomic ratio of Pt/Zn was about 2, while that of Pt/In changed from 2 to 7. It is suggested that formation of a PtZn phase in the former and a Pt_3In in the latter is possible.

3.2. Electrical resistivity changes

Fig. 3a shows the variation of electrical resistivity with temperature in the solution-treated alloy during continuous heating at a rate of 0.5 °C min^{-1}. Upon heating the resistivity begins to decrease at about 310 °C. After attaining a bottom, it increases again, followed by a small change in slope at about 740 °C. This behavior can be seen more clearly on the $d\rho/dT - T$ curve as shown in Fig. 3b. These changes suggest that some phase transformation in the present alloy occurs in two stages (I and II) during the heating. Stage I is the main

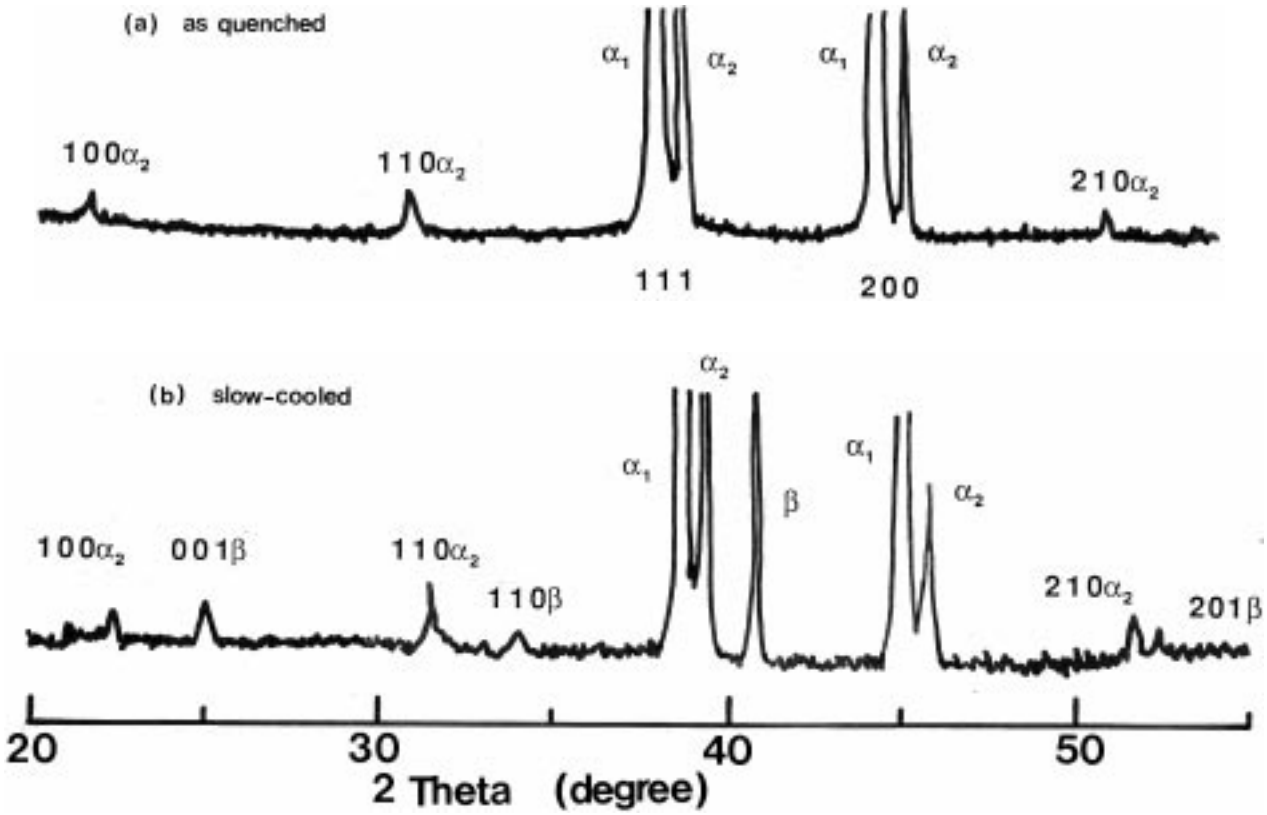

Figure 2 XRD profiles in the specimens (a) quenched from 800 °C and (b) slowly cooled to room temperature.

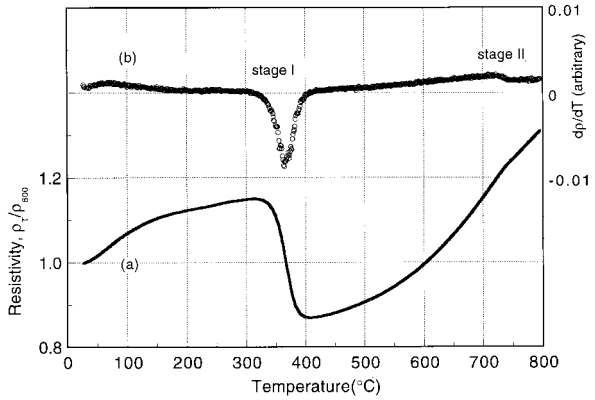

Figure 3 Variation of electrical resistivity and its temperature derivatives during continuous heating at a rate of 0.5 °C min^{-1} in the specimen solution-treated at 800 °C for 1 h and quenched.

transformation phase and has a simple reaction mode. It is considered that stage II corresponds to an equilibrium reaction from three phases $(\alpha_1 + \alpha_2 + \beta)$ to two phases $(\alpha_1 + \alpha_2)$, comparing the data in the above section.

Fig. 4 shows the variations of the anisothermal annealing curves and their temperature derivatives with different heating rates. A heating-rate dependency for stage I was observed. Using the maximum reaction rate temperatures at each heating scan, a Kissinger plot [15] was constructed and a good straight line was obtained as shown in Fig. 5. The calculated activation energy is 39.3 $\pm$ 1.4 kcal mol^{-1}.

3.3. Hardening behavior

Fig. 6 shows the variation of hardness with temperature during continuous heating at a rate of 0.5 °C min^{-1}. The hardness begins to increase from about 300 °C and attains a peak value at about 410 °C. Thereafter, softening occurs with increasing temperature. Comparing Fig. 6 with Fig. 3a, it seems that the hardness increment is proportional to the output of reaction in stage I.

3.4. Aging reactions

Fig. 7 shows XRD line profile variations in the specimen: (a) as-quenched from 800 °C, (b) subsequently heated to 400 °C and (c) 600 °C at a rate of 0.5 °C min^{-1}. As pointed out in Section 3.1, the solution-treated specimen consists of two-phases $(\alpha_1 + \alpha_2)$ having fcc and ordered fcc structures. Fig. 7b corresponds to stage I, which produced remarkable hardening as can be seen in Fig. 6. At 400 °C, new peaks with significant broadening around $2\theta = 40.5$ and 138.5° could be detected, though the peaks from the matrix (α_1 and α_2 phases) obviously remain. This precipitation must produce the hardening. The peaks were identified as an fct ordered β phase and an fcc α_1 phase. Thus, this suggests coexistence of the matrix material and the precipitate. With elevating the temperature, the precipitate seems to develop and the matrix disappears as shown in Fig. 7c. At this stage, we can detect the 1 1 1 reflection of the α_2 phase in the precipitates around $2\theta = 39.2°$, because of development of the reaction and the disappearance of the matrix. The XRD profile indicates the sharpening which resulted in a hardness softening as seen in Fig. 6.

Fig. 8 shows SEM images of the specimen during continuous heating at a rate of 0.5 °C min^{-1}. Fig. 8a reveals that the microstructure at 800 °C consists of two phases, namely white particles and others. This is in good agreement with the results of XRD analyses. With elevating temperature, very fine precipitates seem to occur in the black regions, as can be seen in Fig. 8b and c. At 700 °C, growth of the precipitates is observed, as can be seen in Fig. 8d. We can recognize that the precipitates have a noduler structure, about 230 nm thick. The

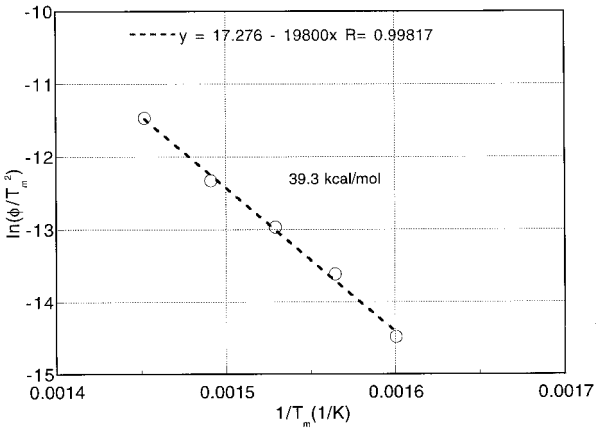

Figure 5 Kissinger plot for stage I.

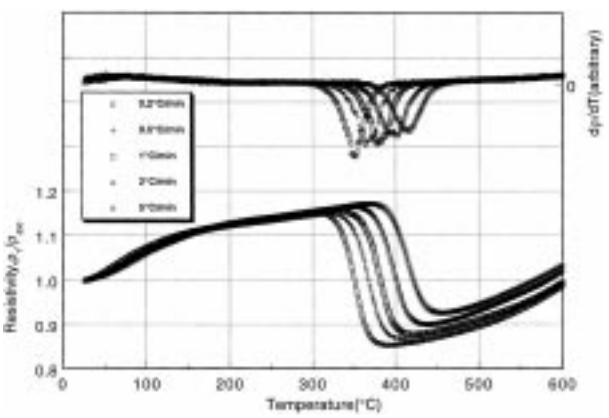

Figure 4 Variation of electrical resistivity and temperature derivatives during continuous heating with different rates in the specimen solution-treated at 800 °C for 1 h and quenched.

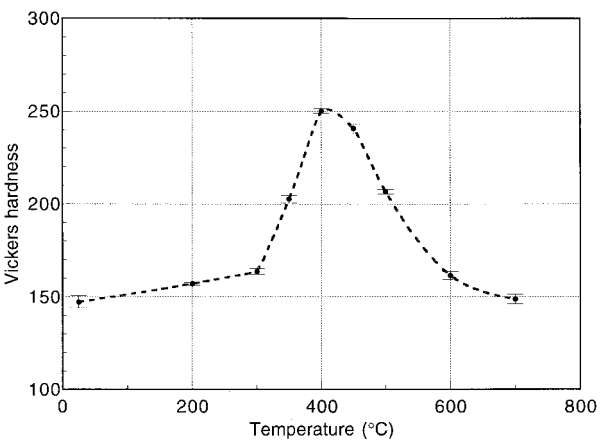

Figure 6 Variation of micro-Vickers hardness with temperature during continuous heating at a rate of 0.5 °C min^{-1}.

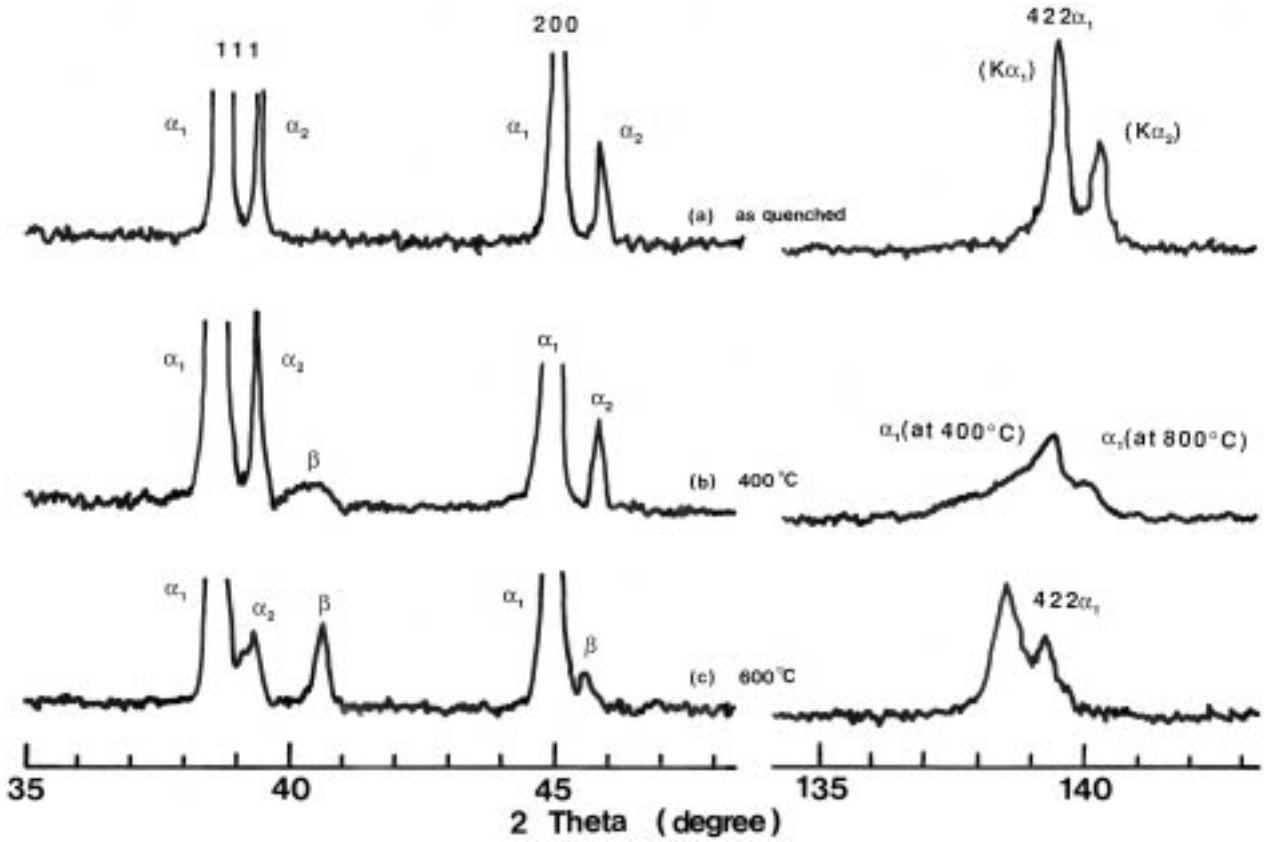

Figure 7 XRD profiles of the specimen: (a) as-quenched from 800 °C, (b) subsequently heated up to 400 °C and (c) 600 °C at a rate of 0.5 °C min $^{-1}$.

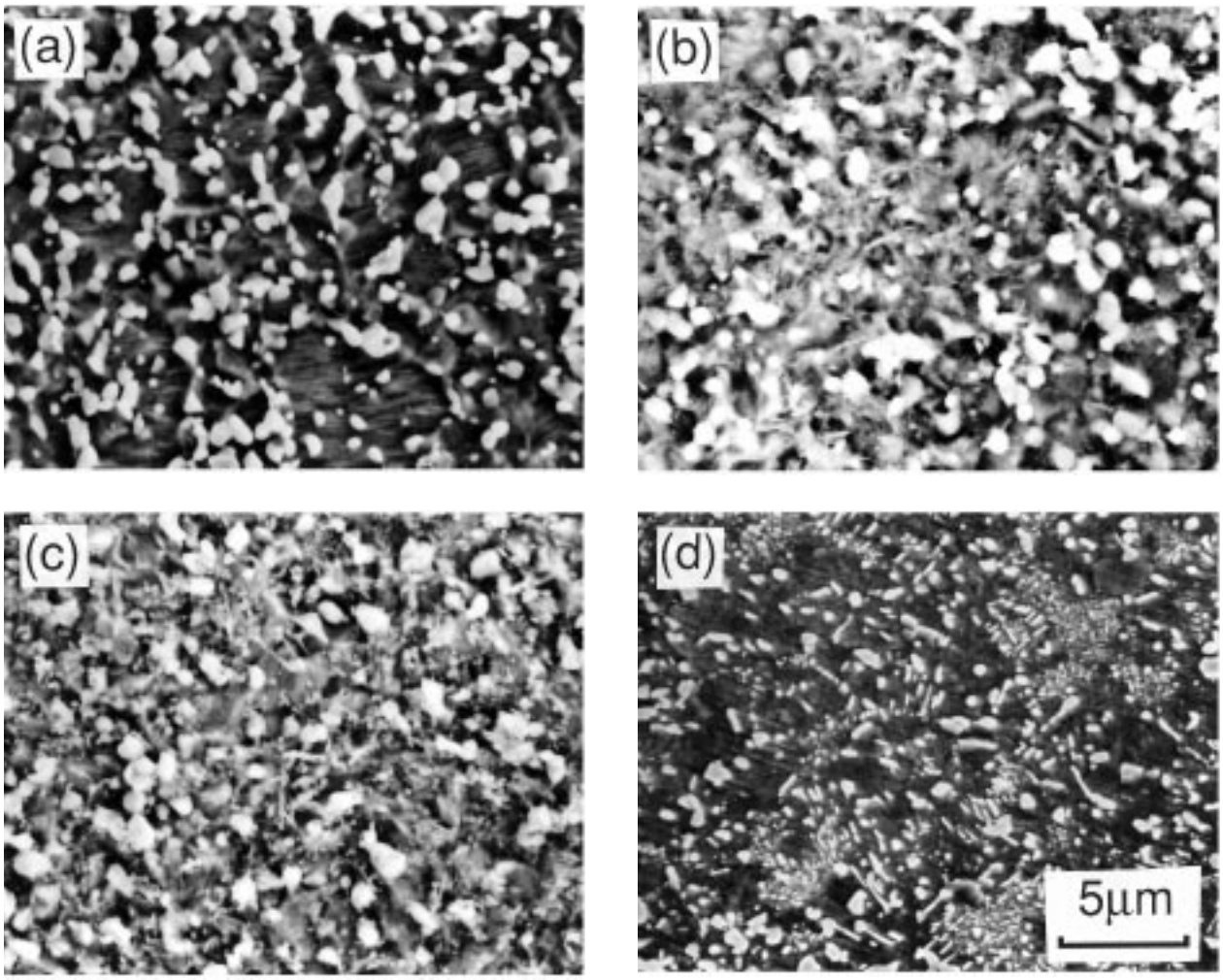

Figure 8 SEM images of the specimen: (a) as-quenched from 800 °C, subsequently heated up to (b) 400 °C, and (c) 600 °C and (d) 700 °C.

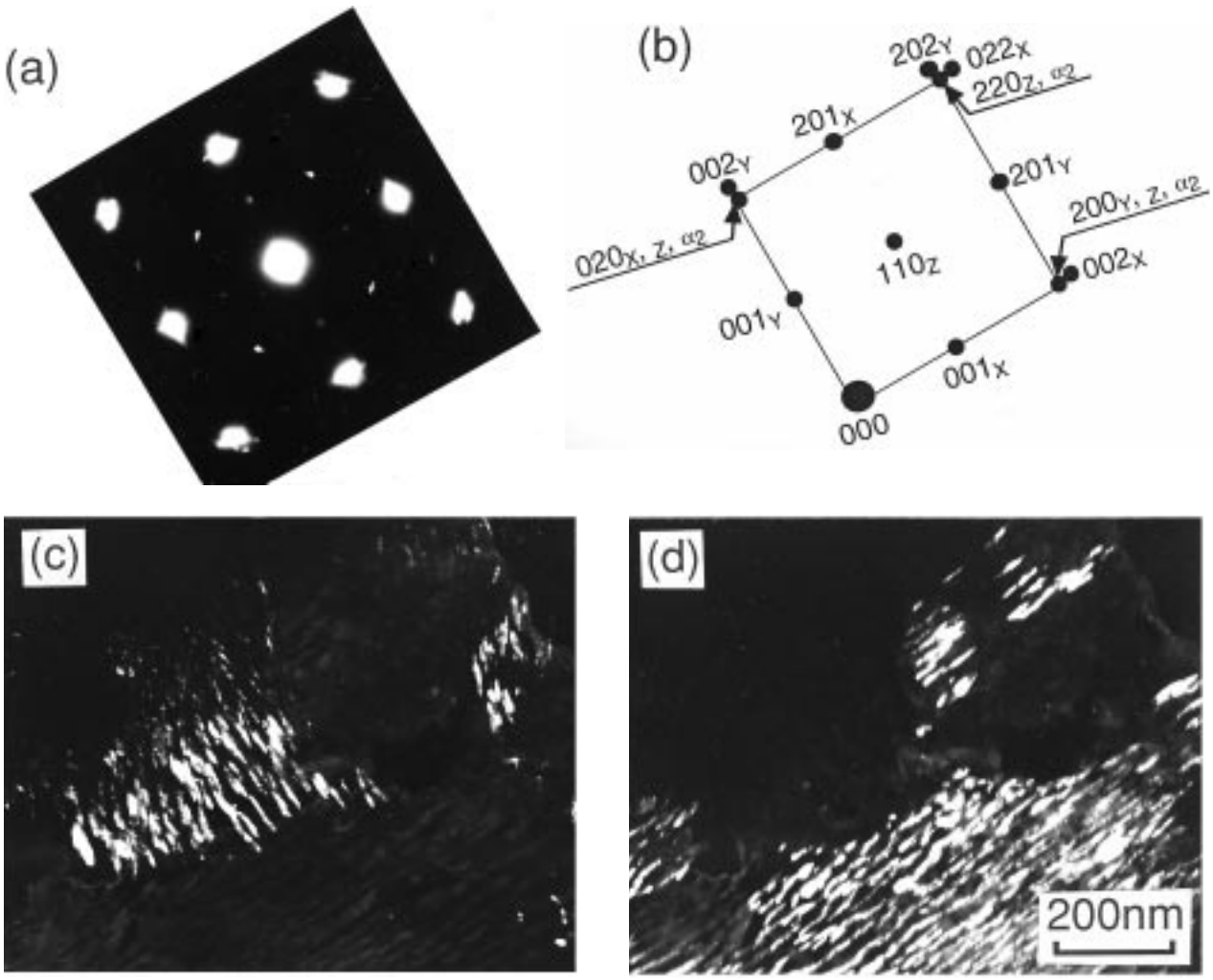

Figure 9 (a) Selected-area diffraction pattern with [0 0 1] incidence, (b) its key diagram, (c) $0\,0\,1_x$ and (d) $0\,0\,1_y$ dark field images of the specimen heated up to 400 °C at a rate of 0.5 °C min^{-1} and quenched.

nodules cover the entire surface of the grains and result in a softening. Such characteristics have been reported in many dental gold alloys [1–7]. The very fine precipitates were analyzed by TEM. Fig. 9 shows: (a) a selected-area diffraction pattern with [0 0 1] incidence; (b) its key diagram; (c) $0\,0\,1_x$ and (d) $0\,0\,1_y$ dark field images of the specimen heated up to 400 °C at a rate of 0.5 °C min^{-1} and quenched, at the temperature of which a hardness peak was obtained, as seen in Fig. 6. This reaction corresponds to stage I. Diffraction analysis proves that an fct ordered β structure with three orientation variants (*x*, *y* and *z*) was produced, the same as seen in Fig. 7b by XRD. It is noticed in the dark field images of Fig. 9c and d that the precipitates are composed of very fine nodules. The average width was about 10 nm, which is about one-twentieth of the grown nodule as seen in Fig. 8d. Such very fine nodular precipitation can cause hardening, as reported in Pd–Cd [16], Cu–Cd [17], Cu–Ag [18], Co–W [19] and dental gold [7] alloys. The apparent activation energy in stage I was 39.3 kcal mol^{-1}, as mentioned above. The formation of a β phase (PtZn) seems to play the most important role in stage I. Zinc is a very diffusional element. Therefore, the value may correspond to the migration of Pt atoms, although we have no diffusion data available for such a multicomponent alloy. It is plausible that Ascoli *et al*. [20] and Baccella *et al*. [21] have reported 32.7 and 34.1 kcal mol^{-1}, respectively, as the migration energy for pure Pt.

4. Conclusions

Phase transformation of a multipurpose dental casting gold alloy during continuous heating was studied by electrical resistivity measurements, hardness tests, XRD, SEM and TEM. A discontinuous precipitate with very fine nodules produced remarkable hardening. The multipurpose alloy used in the present study is characterized by the introduction of a PtZn phase instead of a CuAu I phase, both of which have $L1_0$ structure.

References

1. K. HISATSUNE, M. OHTA, T. SHIRAISHI and M. YAMANE, *J. Dent. Res.* **61** (1982) 85.
2. *Idem*., *J. Less-Common Metals* **83** (1982) 243.
3. K. HISATSUNE, M. NAKAGAWA, K. UDOH, B. I. SOSROSOEDIRDJO and M. HASAKA, *J. Mater. Sci. Mater. Med.* **1** (1990) 49.
4. K. HISATSUNE, K. UDOH, M. NAKAGAWA and M. HASAKA, *J. Less-Common Metals* **160** (1990) 247.
5. K. HISATSUNE, M. HASAKA, B. I. SOSROSOEDIRDJO and K. UDOH, *Mater. Char.* **25** (1990) 177.
6. K. HISATSUNE, Y. TANAKA, T. TANI and K. UDOH, *J. Mater. Sci. Mater. Med.* **3** (1992) 54.
7. K. HISATSUNE, Y. TANAKA, K. UDOH and K. YASUDA, *ibid.* **8** (1997) 277.
8. N. ANDOH, M. TANNO, R. INAGAKI, Y. TAKADA and O. OKUNO, *J. Dent. Tech.* **22** (1994) 1085.
9. *Idem*., *ibid.* **22** (1994) 1177.

10. Y. TAKADA, K. IIJIMA, O. OKUNO, K. SASAKI, M. YODA, K. KIMURA, M. TANNO, R. INAGAKI and N. ANDO, *Tohoku Univ. Dent. J.* **14** (1995) 68.
11. R. INAGAKI, M. TANNO, N. ANDO, Y. TAKADA, K. IIJIMA, O. OKUNO, T. KONNO, K. SASAKI, M. YODA and K. KIMURA, *ibid.* **14** (1995) 216.
12. H. NOWOTNY, E. BAUER, A. STEMPFL and H. BITTNER, *Monatsch. Chem.* **83** (1952) 221.
13. K. C. JAIN and S. BHAN, *Trans. Indian Inst. Met.* **25** (1972) 100.
14. W. CARL and K. SCHUBERT, *J. Less-Common Metals* **19** (1969) 279.
15. H. E. KISSINGER, *Anal. Chem.* **29** (1957) 1702.
16. R. NOZATO, *J. Jpn. Inst. Metals* **24** (1960) 196.
17. H. G. SCHLÖSSER and G. WASSERMANN, *Z. Metallk.* **41** (1950) 162.
18. T. KAINUMA and R. WATANABE, *J. Jpn. Inst. Metals* **33** (1969) 198.
19. J. DUTKIEWICZ and G. KOSTORZ, *Acta Metall. Mater.* **38** (1990) 2283.
20. A. ASCOLI, M. ASDENTE, M. GERMAGNOLI and MANARA, *J. Phys. Chem. Solids* **6** (1958) 59.
21. G. L. BACCELLA, E. GERMAGNOLI and S. GRANATS, *J. Appl. Phys.* **30** (1959) 748.

Received 20 November 1997
and accepted 31 August 1998